Analysis of large-scale structures in turbulent plane Couette flow at low friction Reynolds number

Sergio Gandía-Barberá[1]

Escuela Técnica Superior de Ingeniería del Diseño
Universitat Politècnica de València, Valencia, Spain

Abstract

The presence of large-scale roll-like structures in turbulent plane Couette (C-) flow has been proven experimentally and numerically in the last decades. This kind of flow is purely shear-driven. Curiously enough, these structures are not present in pressure-driven flows such as turbulent plane Poiseuille (P-) flow. In this paper the large-scale structures (LSS) in turbulent plane Couette flow are studied at the low friction Reynolds number $Re_\tau = 125$ through DNS in a channel domain. A stepped transition from turbulent plane Couette flow to turbulent plane Poiseuille flow is covered in order to analyse the properties of the flow during this transition. The length and width of these large-scale coherent motions are estimated $50h$ and $2.3h$ respectively, being h the semi-height of the channel domain. It is proven that the streamwise LSS structures develop very-long counter-rotating rolls in the mean flow. The presence of the rolls is linked to the distribution of Reynolds stress along the wall-normal direction.

Keywords: Numerical turbulence, DNS, Couette flow, Poiseuille flow

1. Introduction

Inside the wide subject of Fluid Mechanics there is a relevant branch, which studies the unsteady, irregular and chaotic movement of the flow. This branch is called turbulence. Turbulent flows are present in most of our daily life situations: from the fumes in a chimney to almost every aerospace engineering problem.

Broadly speaking, one can assess if a flow is turbulent by estimating its Reynolds number. This non-dimensional number described in Eq. 1 compares the inertial forces (numerator) to the viscous forces (denominator) of the flow. At low Reynolds numbers, viscous forces are dominant, developing a smooth flow known in Fluid Mechanics as laminar. On the contrary, at high Reynolds numbers the predominant inertial forces produce chaotic eddies and flow instabilities; that is, a turbulent flow.

$$Re = \frac{\rho u L}{\mu} = \frac{uL}{\nu} \tag{1}$$

where:

- ρ is the density of the fluid $\left[kg/m^3\right]$
- u is the velocity of the fluid with respect to an external observer $[m/s]$
- L is a characteristic linear dimension $[m]$
- μ is the dynamic viscosity of the fluid $[kg/(m \cdot s)]$
- ν is the kinematic viscosity of the fluid $\left[m^2/s\right]$

In Fluid Mechanics it is often relevant to estimate the velocity field as well as the flow characteristics in a given 2D or 3D domain in order to gain a better understanding of a case. These parameters are nowadays calculated through the Navier-Stokes (N-S) equations, which were developed in the beginning of the XX century. In Eq. 2 the Navier-Stokes equations for an incompressible case are depicted. They are complemented with the continuity equation, which for incompressible flow breaks down to $\nabla u_i = 0$.

[1]MSc in Aerospace Engineering, serganba@etsid.upv.es

$$\frac{\partial u_i}{\partial t} + u_j \frac{\partial u_i}{\partial x_j} = -\frac{1}{\rho}\frac{\partial p}{\partial x_i} + \nu \frac{\partial^2 u_i}{\partial x_j^2} \tag{2}$$

Note that i and j are subscripts referred to Einstein summation convention. Hence, Eq. 2 contains in fact three different equations, one for each dimension.

The resolution of Navier-Stokes equations for a turbulent flow is still these days a great challenge due to their complex non-linear form. Three different schemes have been developed with regard to their level of resolution precision: RANS, LES and DNS.

DNS (Direct Numerical Simulation) is employed in this study in order to calculate the velocity fields of turbulent plane Couette and Poiseuille flows. In this scheme the N-S are solved numerically without any approximation. Hence, its main advantage is the high precision of the results, which is specially convenient in scientific studies. On the other hand, the computational cost is very high and dependent on the simulation Reynolds number. This limitation allows these days only to simulate up to moderate Reynolds numbers in very simple geometries, usually called canonical domains. For more information about the resolution methods of the Navier-Stokes equations, the interested reader is referred to the classic book of Pope [1], Part Two.

Since the seminal paper of Kim, Moin and Moser [2] turbulent channel flows have been widely studied through direct numerical simulation (DNS). In this domain the turbulence regime is defined by the friction Reynolds number, $Re_\tau = u_\tau h/\nu$, where u_τ is the friction velocity, and h is the semi-height of the channel.

Channel Poiseuille flows have been studied at higher friction Reynolds numbers than Couette flows due to the existence of very large-scale roll-like motions (LSS) extending along the domain. This fact results in the necessity of long and wide channels in order to capture the LSS. Hence, C-flows are more computationally expensive than P-flows at the same Reynolds number.

Couette flow is a classical problem of primary importance in the history of fluid mechanics. It is widely studied among students, as laminar C-flow develops an exact solution for N-S equations. Couette flow describes the flow of a viscous fluid in the space between two surfaces. Generally the bottom surface remains static and the top surface moves with a constant velocity. Hence, the flow is driven by the shear force acting on the fluid due to the relative movement of the upper wall. A pressure gradient in streamwise direction is normally not applied.

Despite being one of the simplest viscous flows, it retains much of the same physical characteristics of more complicated boundary-layer flows. Additionally, it takes place in diverse industrial processes and devices, such as extrusion, power generators and pumps. [3]

On the other hand, Poiseuille flow is a classical problem of fluid mechanics too. It describes a steady flow between two parallel plates at a fixed distance. However, the main difference is that both walls are at rest, and the flow movement is caused by an external negative pressure gradient in streamwise direction. This flow is therefore considered a pressure-driven flow. Poiseuille flow is widely employed in the industry to study pipeline flow.

As stated in the abstract, in this paper a transition from turbulent plane C-flow to P-flow is studied through DNS simulations in a channel domain. Simulations are done at $Re_\tau = 125$. Pure Couette flow simulations at this low Reynolds number are therefore comparable to other simulations made by Bernardini et al. [4] and Tsukahara et al. [5], among others.

The aim of this study is to observe and measure the dimensions of the large-scale structures (LSS) at C-flow and during the transition. Additionally, we try to understand how flow characteristics change when LSS are present by comparing with a pure P-flow.

The structure of the paper is as follows. In the second section, the simulation domain with its boundary conditions as well as the simulation cases are presented. In the third section, LSS are introduced and described by depicting streamwise velocity fields from the simulation results. In the fourth section, vortices in diverse domain regions are compared among simulation cases. Finally, the fifth section contains the summary and conclusions.

2. Simulation cases and boundary conditions

The stepped transition from pure C-flow to pure P-flow was performed in a very long computational channel. The transition cases (C-P flow) have both pressure gradient and a relative top wall movement in comparison with the bottom wall. The domain dimensions are $L_x = 128\pi h$, $L_y = 2h$, and $L_z = 6\pi h$, being x, y, z the streamwise, wall-normal and spanwise direction, respectively. Their corresponding velocity components are U, V, and W. Defining the average operator $\langle\cdot\rangle_{x_i}$ as

$$\langle\phi\rangle_{x_i} = \frac{1}{L_{x_i}\,(t_1 - t_0)} \int_{t_0}^{t_1} \int_0^{L_{x_i}} \phi \, dx_i \, dt \tag{3}$$

the value of $\langle\phi\rangle_x$ can be thought as the mean in x of the time-averaged field of parameter ϕ. Statistically averaged quantities are denoted by an overbar, $\overline{\phi} = \langle\phi\rangle_{xz}$ whereas fluctuating quantities are denoted by lowercase letters, i.e., $U = \overline{U} + u$. The semi-height of the channel is referred as h. Note that wall-normal dimension extents from $-h$ (bottom wall) to h (top wall).

A graphical description of the domain is depicted in Figure 1. Furthermore, a small channel of $L_x = 16\pi h$, $L_y = 2h$, and $L_z = 6\pi h$ was used in order to observe the influence of the channel domain.

The use of a very long channel stems as a conclusion from previous studies at similar Reynolds numbers, in which shorter domains were employed. Bernardini [4] studied a pure C-flow at $Re_\tau = 167$ in a channel $(12\pi h \times 2h \times 4\pi h)$. Tsukahara [5] performed a similar study at $Re_\tau = 126$ in diverse channels up to $(64h \times 2h \times 4\pi h)$. Despite in these studies relevant conclusions were stated, due to the length of the domain the LSS could not be measured properly.

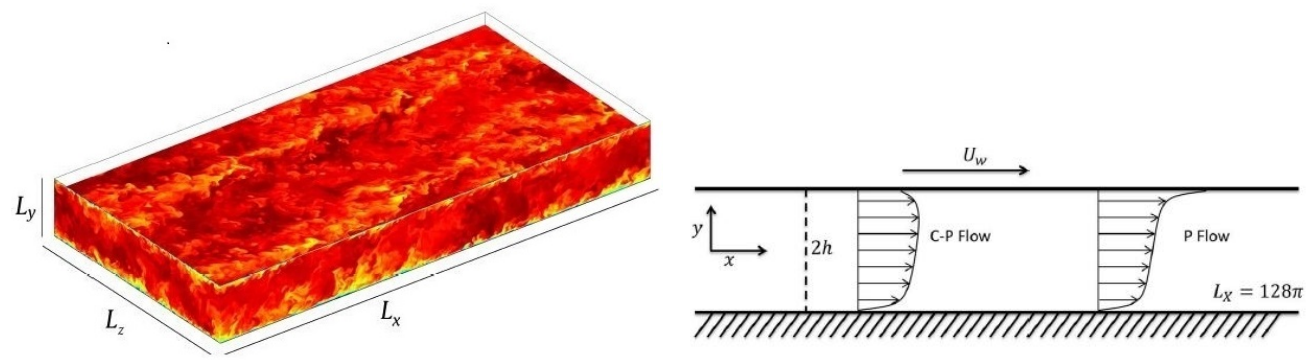

(a) (b)

Figure 1: a) Descriptive 3D view of a channel domain. b) Schematic 2D view of a channel domain. The flow moves from left to right along X direction. In case of C-flow the top wall moves in streamwise velocity. In both cases the domain dimensions are not scaled.

The boundary condition set in stream- and spanwise limiting walls is periodicity. This kind of boundary condition does not affect directly the velocity components of the flow. However, it is proven that periodical boundaries increase the coherence of LSS if the length of the domain is too short [6]; that is, clearly shorter than the LSS length. See Figure 2h.

On the other hand, in the wall-normal direction no-slip and no-penetration boundary conditions are present. In C-flow the top wall moves additionally in streamwise direction at a constant velocity U_w. In P-flow both walls are at rest.

The flow can be described by means of the momentum and mass balance equations. These equations are solved using the LISO code, which has successfully been employed to run some of the largest simulations of turbulence [7], [8]. In wall units, the simulation resolution in wall-normal direction Δy^+ varies from 0.83 at the wall, up to 2.3 at the centerline. The wall-parallel resolution in physical space for x and z is $\Delta x^+ \simeq 8.4$ and $\Delta z^+ \simeq 4.3$.

The characteristics of the simulation cases are summarized in Table 1. The employed nomenclature describes the percentage of C-flow and P-flow of each case; that is, C10P00 is pure C-flow. In each case the same bulk Reynolds number, based on the bulk velocity U_b, is conserved.

Case	Line	Re_τ^m	Re_τ^s	N_x	N_y	N_z	TU_b/L_x	Tu_τ/h
C10P00	—o—	132	132	6144	151	576	8.9	188
C08P02	······	133	83	6144	151	576	10.9	235
C06P04	– – – –	135	13	6144	151	576	11.2	243
C04P06	—·—	137	69	6144	151	576	19.4	430
C02P08	——	142	102	6144	151	576	16.8	384
C00P10	—■—	147	147	6144	151	576	11.1	264

Table 1: Parameters of the simulations. Two different Reynolds numbers are given depending on the local u_τ at the moving (third column) or the stationary (fourth) wall. N_x, N_y, N_z are the collocation points in physical space. The last two columns denote the computational time span while statistics were taken in wash-outs (U_b/L_x) and eddy turn-overs (u_τ/h). T is the computational time spanned by those fields. Line shapes given in the second column are used to identify the cases through all the figures of the present paper.

3. Large Scale Structures (LSS) in C-flow

The presence of large scale structures in the flow is assessed by observing and measuring the velocity fields in the domain. As stated in previous studies ([5], [9], [10]) the LSS occupy almost all the wall-normal dimension of the domain, and extend along the streamwise direction.

Therefore, we compare first the streamwise velocity on a plane in the channel center of the small domain. The comparison is made along the transition cases from pure P- to C-flow. For the sake of clarity, for each case the mean and instantaneous U fields are shown. Second, the time and streamwise average $\langle U \rangle_x$ is plotted in a YZ plane for each transition case; through these images we can observe their wall-normal extent. Third, through analysis tools the length and width of the LSS is calculated during the transition.

In Figure 2 filtered streamwise velocity fields at instantaneous simulation times are depicted on the left. As one can read in each caption, these figures start from case C00P10 (pure Poiseuille) on the top to C10P00 (pure Couette) on the bottom. The filtering algorithm employed is described in [11], Section 4.6. The filtering threshold is the standard deviation among all streamwise velocity values in the selected wall-parallel plane. See that now one can differentiate between three zones of colour:

- **Yellow**: high-speed regions, where local streamwise speed is above the standard deviation.
- **Light blue**: neutral regions, where local streamwise speed is inside the range of the standard deviation.
- **Dark blue**: low-speed regions, where local streamwise speed is below the standard deviation.

On the right column, the mean streamwise velocity of each case is depicted without filtering. This magnitude helps to find patterns visible after averaging many instantaneous fields.

As we can see in Figure 2, in pure Poiseuille the filtered streamwise velocity structures (Figure 2a) arrange in a total random organization. The filtered field is composed by short and scattered structures. So, we can see that low-speed and high-speed regions come closer and get away with no clear arrangement. Furthermore, the same lack of organization of the streamwise structures is observed when comparing with the mean streamwise velocity field (Figure 2b).

In instantaneous case C04P06 (Figure 2c) it is observed for the first time that structures of the same kind start to organize creating larger structures than the observed in previous cases. This tendency is confirmed once the mean flow C04P06 in Figure 2d is compared. Nevertheless, it is seen later in Figure 3 that LSS are not developed yet.

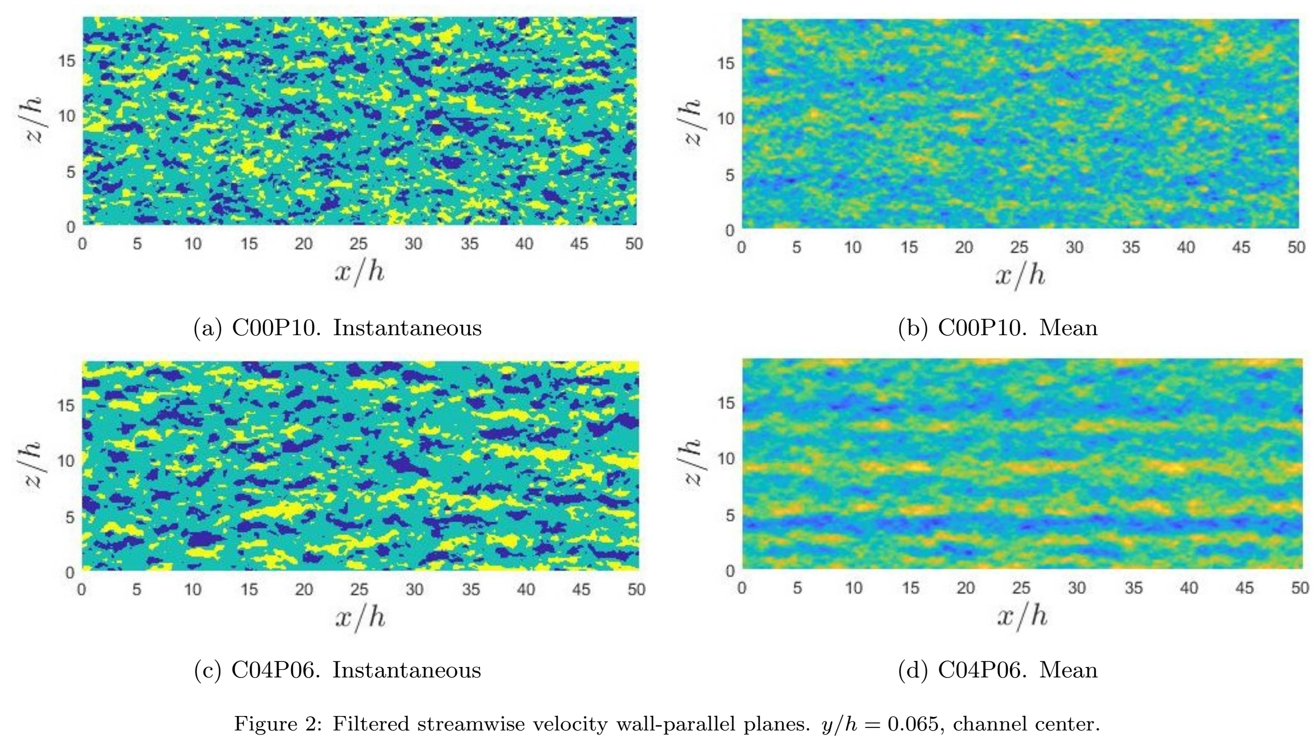

(a) C00P10. Instantaneous

(b) C00P10. Mean

(c) C04P06. Instantaneous

(d) C04P06. Mean

Figure 2: Filtered streamwise velocity wall-parallel planes. $y/h = 0.065$, channel center.

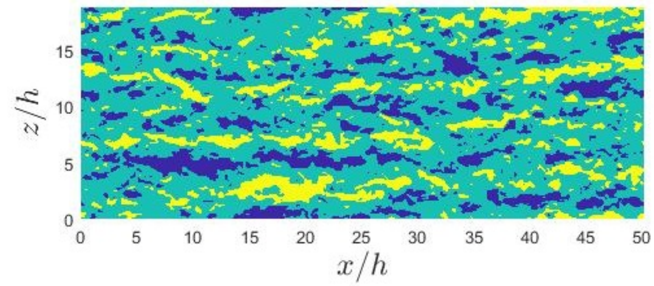

(e) C06P04. Instantaneous

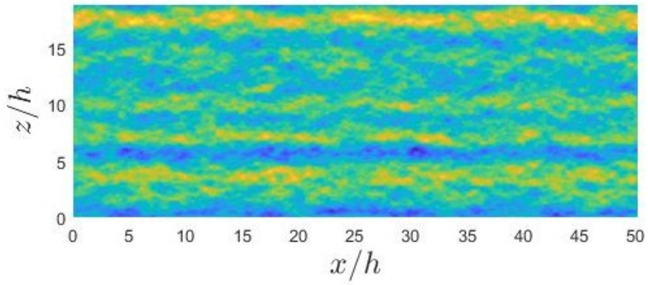

(f) C06P04. Mean

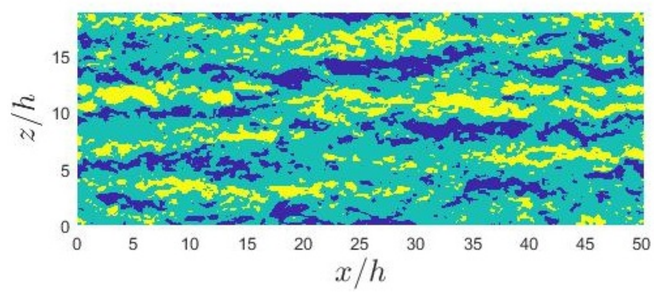

(g) C10P00. Instantaneous

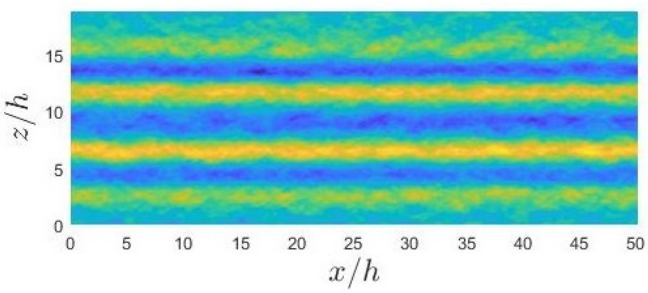

(h) C10P00. Mean

Figure 2: Filtered streamwise velocity wall-parallel planes. $y/h = 0.065$, channel center.

In instantaneous case C06P04 (Figure 2e) the level of arrangement of the filtered structures increases, observing bigger structures than the initial ones at C00P10 (Figure 2a). By comparing with the mean C06P04 field (Figure 2f) one notices that the structures became stronger (brighter colours) than in the previous cases. However, clear structures extending along the channel streamwise dimension are not developed yet.

Case C10P00 (pure Couette) shows another scenario. Here the filtered streamwise structures (Figure 2g) have completely arranged creating strong structures that touch both streamwise sides of the domain. This feature is clearly noticed in the mean C10P00 field (Figure 2h), in which each kind of structure is perfectly organized. An alternating pattern is described: high-, neutral and low speed regions. Additionally, all structures touch both limiting sides in streamwise direction.

The next step is to observe this transition in a YZ plane, in which a streamwise and temporal average $\langle U \rangle_x$ has been performed. This is depicted in Figure 3 for the same cases as in Figure 2. Notice that now there is no instantaneous field depicted, and the small channel domain was employed.

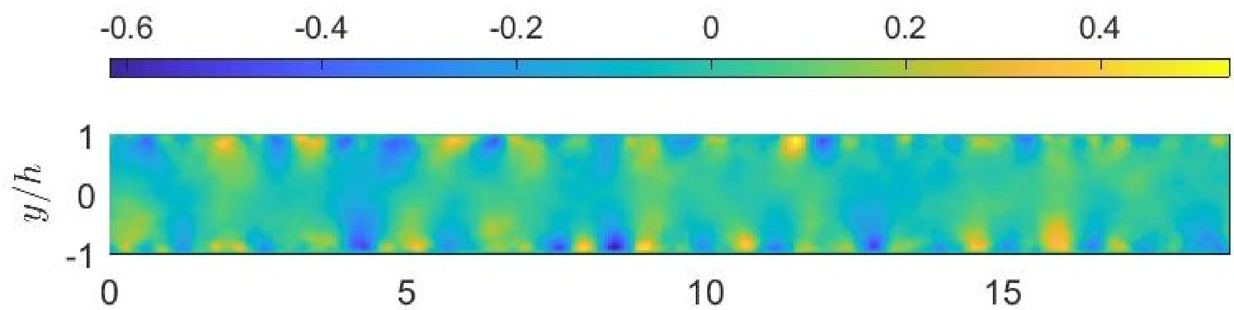

Figure 3: Time- and streamwise-averaged images of u/u_τ for the cases, top to bottom, C00P10, C04P06, C06P04 and C10P00

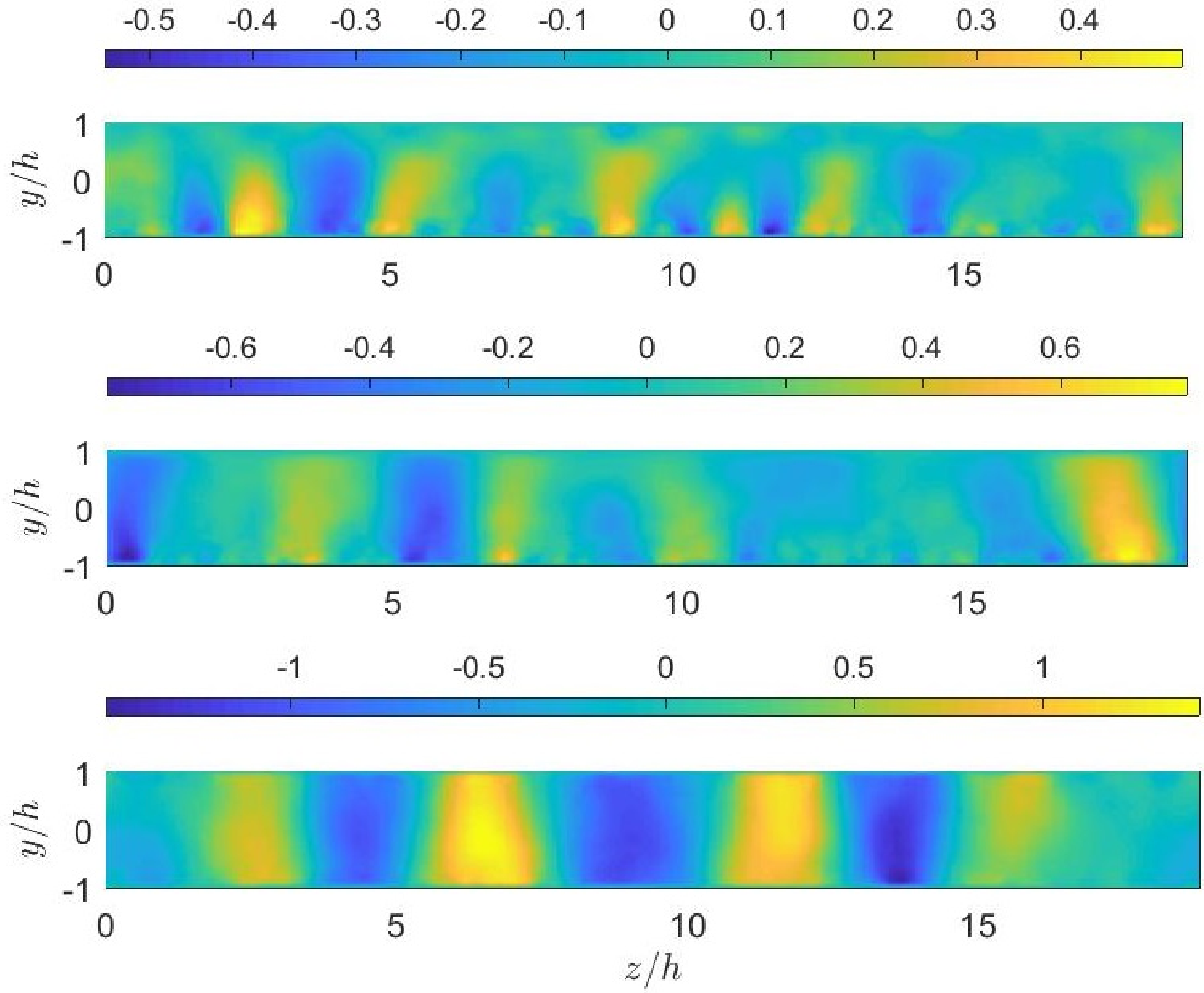

Figure 3: Time- and streamwise-averaged images of u/u_τ for the cases, top to bottom, C00P10, C04P06, C06P04 and C10P00

In the pure P-flow (C00P10) an alternating pattern of high- and low-speed structures near both walls is observed. However, the averaged streamwise velocity in the channel center is around zero. This occurs due to the random distribution of structures observed in Figure 2a.

As soon as we reach intermediate states C04P06 and C06P04, the structures increase its height from the stationary wall (bottom) to the moving wall (top).

Finally, at pure Couette C10P00 the alternating pattern of streamwise velocity structures occupy the whole height of the channel, and the whole length (Figure 2h) in the small channel. From this result stems the necessity of employing a very-long computational domain in order to catch the length of LSS at the simulated Reynolds number. Simulations were run therefore in a very-long computational domain as described in Table 1.

Up to now we notice that LSS forming counter-rotating rolls are present up to case C06P04. In Gandía-Barberá et al. [8] the presence of rolls was linked to the distribution of the Reynolds stress $\langle uv \rangle_{xz}$. The authors stated that as soon as the Reynolds stress crosses the zero value, these structures fade away. From C06P04 to C10P00 the Reynolds stress $\langle uv \rangle_{xz}$ holds a negative value along the wall-normal dimension.

Before getting deeper into dimension analysis, in an interesting study Lee and Kim [12] described for a pure Couette flow in a similar domain the same alternating distribution as in Figure 3. The authors compared this distribution with a vector field composed by $\langle v \rangle_x$ and $\langle w \rangle_x$.

This idea was later employed in a similar study performed in a still unpublished paper by Alcántara et al. [13]. In this work the authors studied a pure thermal Couette flow at $Re_\tau = 476$ in a domain of size $(L_x, L_y, L_z) = (16\pi h, 2h, 6\pi h)$. The same wall-normal distribution of LSS as in Figure 3 is observed for a time- and streamwise averaged u velocity, named as $\langle u \rangle_x$. This is depicted in Figure 4.

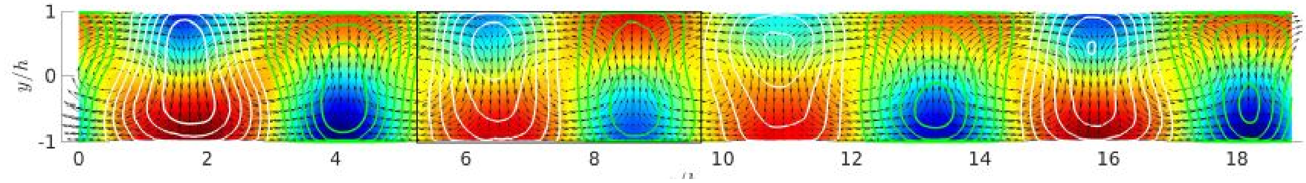

Figure 4: Time- and streamwise averaged temperature field in a YZ plane. White and green lines represent contours of positive and negative $\langle u \rangle_x$, respectively. ($\langle v \rangle_x$, $\langle w \rangle_x$) vector field is represented by arrows.

Notice that in each high- or low-speed structure two counter-rotating velocity rolls touch each other. The rotation axis of each roll is located in the transition between high- and low-speed structures in the channel center. The black box depicted in Figure 4 encloses a pair of $\langle u \rangle_x$ structures, and a roll in its center. By comparing this finding with Figure 2h one can realize that the averaged velocity field shows long counter-rotating rolls that extend along the streamwise dimension of the domain.

On the other hand, notice that the thermal distribution in a C-flow (Figure 4) describes a pair of hot (red) and cold (blue) regions at each velocity structure. At a given roll these thermal structures describe a symmetry with respect to the origin of every (v, w) vortex. This symmetry is described for the first time in Alcántara et al. [13].

In order to measure the length and width of the streamwise structures that form these rolls a two-points correlation in the channel center is employed in each transition case. The correlation is applied in streamwise and spanwise direction in order to measure the length and width of the counter-rotating rolls, respectively.

Two-points correlation R_{ij} is a mathematical tool commonly employed in the literature in order to find repeating patterns, such as the presence of a periodic signal obscured by noise, or identifying a fundamental frequency.

The possible values for R_{ij} lie in the range $[-1, 1]$, with 1 indicating perfect correlation and -1 indicating perfect anti-correlation. Do not confound anti-correlation (-1) with no correlation between values, in which R_{ij} becomes 0. For more information, the interested reader is referred to [1] Section 6.3, or to [11] Section 5.3.

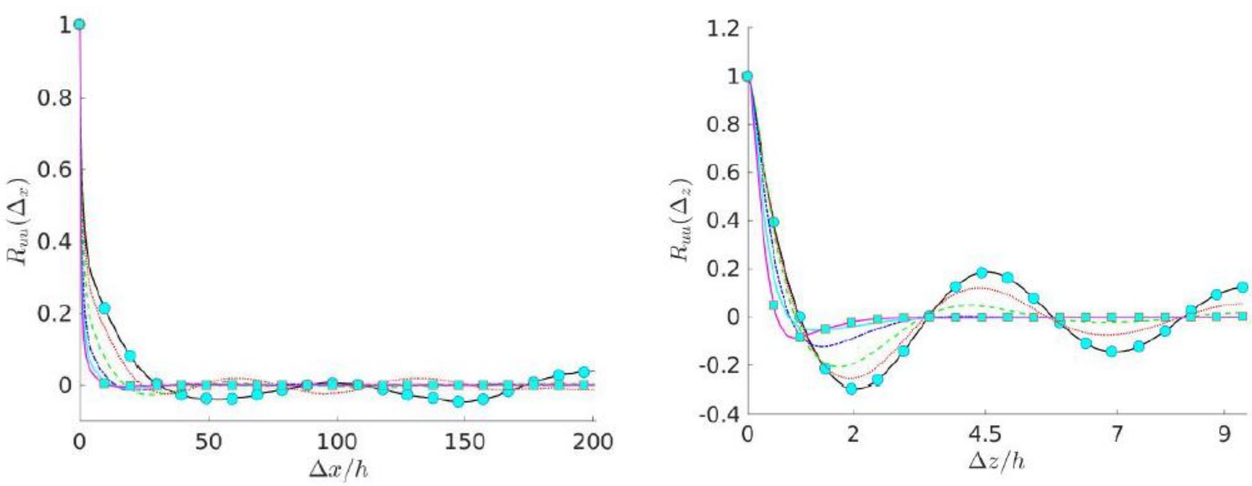

(a) (b)

Figure 5: Colors as in Table 1. Two-points correlation of U evaluated at the channel center in a) streamwise and b) spanwise direction. The length of the domain is $128\pi h$.

The length of the counter-rotating rolls is measured from Figure 5a as half of the distance between two consecutive minima of the curve. For the pure C-flow case it is measured as $50h$, approximately. This measure could not be extracted in previous studies ([10], [5]) due to the insufficient length of their domain.

The length of the LSS gets shorter as soon as the Couette contribution is reduced; that is, from case C08P02. This feature can only be observed by using a very-long channel domain. Finally, the different minima cannot be truly appreciated beyond C06P04, as we also stated from Figure 2.

In an interesting study M. Lee and Moser [9] performed two-points correlations in a box of length $100\pi h$ for Couette flows at $Re_\tau = 220$ and $Re_\tau = 500$. For the former case, the authors calculated that streamwise structures have a length of $25\pi h$; nevertheless, for the latter case the authors could not measure the structures. As a consequence, the authors conclude that the length of LSS is highly dependent on friction Reynolds number.

Recalling the introduction, this dependency puts forward a relevant difficulty since for measuring LSS at higher Re_τ larger domains will be needed. By increasing Re_τ and the domain dimensions, the simulation may become impossible even for current supercomputers.

On the other hand, two-points correlation of U in spanwise direction (Figure 5b) shows that the width of LSS in pure C-flow is $2.3h$, approximately. This value stays in accordance with the results in M. Lee and Moser [9], Avsarkirov et al. [14] and Kraheberger et al. [15]. However, it differs from Tsukahara et al. [5] and Pirozzoli et al. [10]. In these studies the authors estimate smaller values: $1.3h$ and $1.7h$, respectively. The main reason for this discrepancy is the width and length of their domain, which are not sufficient to simulate a full pair of rolls.

Finally, Avsarkirov et al. [14] demonstrated that the LSS width remains constant for pure Couette flows from $Re_\tau = 125$ to $Re_\tau = 550$ in a domain of size $(L_x,\, L_y,\, L_z) = (20\pi h,\, 2h,\, 6\pi h)$. This is also confirmed by M. Lee and Moser [9] in a larger domain at $Re_\tau = 500$. Kraheberger et al. [15] obtained a similar width of the rolls in a pure C-flow at $Re_\tau = 1000$.

Consequently, we conclude that the width of the rolls remains independent of the friction Reynolds number from $Re_\tau = 125$ to $Re_\tau = 1000$, if an appropriate domain size is employed.

4. Analysis of vortex structures

To conclude the analysis of the flow characteristics when LSS are present, the vortex structures are identified and measured for each simulation case. The reason for studying the vortex distribution is to find patterns related to each kind of coherent structure, which are mainly low and high velocity structures.

The vortex identification method used was developed by Chong et al. [16], and it is usually known as Δ criterion. This method is based on a local analysis of the velocity gradient tensor $\nabla\vec{u}$ at each point of the domain. If at a domain point $\vec{x}$ the discriminant Δ of the eigenvalues of $\nabla\vec{u}$ is larger than a given threshold, the identification method classifies that point as a vortex point. For detailed information about the process underlying the method, the reader is referred to Chakraborty et al. [17], in which Δ criterion along with other identification methods is extensively described.

The constant threshold proposed by Chong et al. [16] was later defined as problematic when applied to wall-bounded turbulent flows as in this study. Del Álamo et al. [18] reported the defect of considering a constant threshold in wall-bounded turbulence, owing to the inhomogeneity of the flow in the wall-normal direction. This fact complicates the comparison of data from different wall distances when a uniform threshold is used. When the threshold is chosen to visualize properly the vortices of the near-wall layer of the present channels, very few of them are observed in the outer region. Conversely, when the threshold is lowered to visualize the vortices of the outer layer, the near-wall region becomes confusingly cluttered with vortex tubes. This behaviour is proven to worsen with increasing Reynolds number.

Consequently, Del Álamo et al. [18] proposes a threshold that varies with wall distance with regard to the standard deviation of Δ over wall-parallel planes. See Equation 4. This threshold is higher near the walls than in the channel center; that is, the method is more restrictive with near-wall vorticity.

$$\Delta\left(\vec{x}\right) > \alpha \cdot \overline{\left(\Delta'^2\right)}^{1/2} \tag{4}$$

where α is the percolation limit, which has a constant and different value for each simulated flow.

For the sake of simplicity the algorithms for vortex identification are not explained in this paper. The interested reader is referred to [11], Chapter 4. The percolation limit for each C-P flow is presented in [11], Section 6.1.

The vortex population of each simulation case is analysed in diverse domain regions: near stationary wall, channel center and near moving wall. The aim is to observe how the presence of LSS affects the vortex population.

In this process the vortex points are first identified, second grouped forming vortex clusters, and third the volume of each cluster is measured. All the required algorithms are described in [11], Chapter 4.

The results are processed by employing probability plots of the vortex volumes at each region. This is depicted in Figure 6.

In the near-stationary wall region, all the distributions collapse perfectly. See Figure 6a. This stays in accordance with the fact that streamwise velocity structures located near the stationary wall are analogous among all cases [11], Section 5.2. We conclude that there is a link between the vortex and streamwise structures in this domain region.

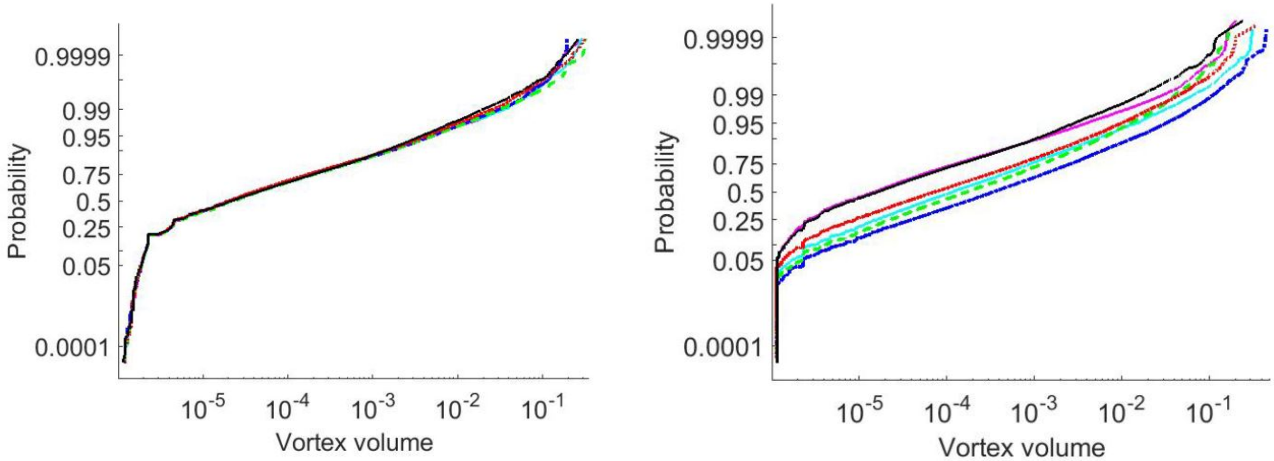

(a) (b)

Figure 6: Colors as in Table 1. Accumulative probability plot of vortex volumes a) near the stationary wall, b) near the moving wall and c) in the channel center. Vortex volumes are divided by h^3. Horizontal axis is in logarithmic units.

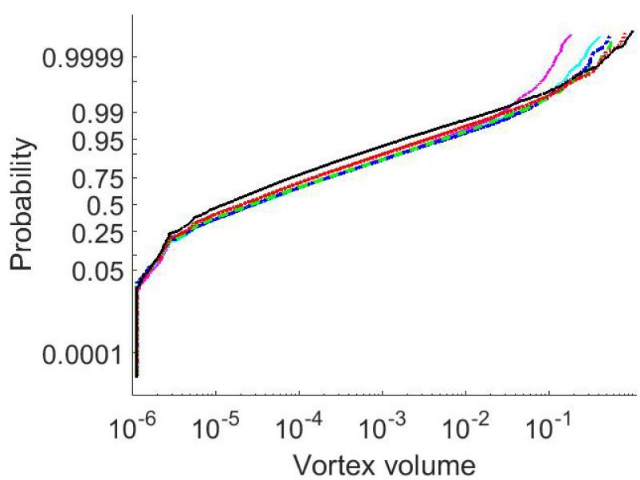

(c)

Figure 6: Colors as in Table 1. Accumulative probability plot of vortex volumes a) near the stationary wall, b) near the moving wall and c) in the channel center. Vortex volumes are divided by h^3. Horizontal axis is in logarithmic units.

In the near-moving wall region (Figure 6b), transition cases show bigger vortices than pure C- or P-flow at a given probability. Curiously enough, pure C- and P-flow distributions collapse perfectly. Recalling the streamwise structures in this region ([11], Section 5.2), we observe that in transition cases rounded structures predominate, specially in C06P04 case. However, pure cases consist on meandering striped structures.

In the channel center (Figure 6c) a good collapse is achieved until vortex volumes reach $0.04h^3$. This fact indicates that the channel center has also a great population of small vortices in all cases. However, it is more interesting to observe the results in Figure 6c once the collapse is lost. Pure Poiseuille flow reaches the maximum accumulative probability in a region near $0.1h^3$. Then, each transition case in a stepped way reaches higher volumes in the channel center. And finally, cases C08P02 and C10P00 collapse at the end of the curves in a region around h^3.

5. Conclusions

A set of transition cases from a pure turbulent Poiseuille flow to a pure turbulent Couette flow were presented in a small and in a very-long channel domain. All simulations were performed at $Re_\tau = 125$.

Streamwise velocity patterns forming large scale structures were detected in pure Couette and transition flows with relevant Couette contribution up to C06P04. These LSS are specially visible in the mean flow. Their presence is also linked to the distribution of the averaged Reynolds stress $\langle uv \rangle_{xz}$.

By comparing with the remaining velocity components in an averaged flow, it is observed that LSS conform counter-rotating rolls that extend along the streamwise direction of the channel. In the small domain these rolls occupy the whole length.

In order to measure the rolls, two-points correlations were employed in stream- and spanwise directions in a very-long channel domain. The length and width of the rolls at $Re_\tau = 125$ are $50h$ and $2.3h$, respectively. From similar studies it is discovered that their length is highly dependent on the friction Reynolds number. Nevertheless, their width shows no dependency on this parameter.

The last step of the analysis was to identify and measure the vortex population in diverse regions of the domain; concretely, near each wall and in the channel center. The vortex volumes in each region show an agreement with the streamwise structures present in each case. When counter-rotating rolls are present in the mean flow, the vortex volumes in the channel center can reach up to h^3.

References

[1] S. B. Pope, Turbulent flows, Cambridge University Press, 2000.

[2] J. Kim, P. Moin, R. Moser, Turbulence statistics in fully developed channels flows at low Reynolds numbers, Journal of Fluid Mechanics 320 (1987) 259–285.

[3] Y. Rihan, Computational study of couette flow between parallel plates for steady and unsteady cases, International Atomic Energy Agency (????).

[4] M. Bernardini, S. Pirozzoli, P. Orlandi, The effect of large-scale turbulent structures on particle dispersion in wall-bounded flows, International Journal of Multiphase Flow 51 (2013) 55–64.

[5] T. Tsukahara, H. Kawamura, K. Shingai, DNS of turbulent Couette flow with emphasis on the large-scale structure in the core region, Journal of Turbulence 7 (2006) 1–16.

[6] J. C. del Álamo, J. Jiménez, Spectra of the very large anisotropic scales in turbulent channels, Physics of Fluids 15 (2003) L41–L44.

[7] S. Hoyas, J. Jiménez, Scaling of the velocity fluctuations in turbulent channels up to $Re_\tau = 2003$, Physics of Fluids 18 (2006) 011702.

[8] S. Gandía-Barberá, S. Hoyas, M. Oberlack, S. Kraheberger, Letter: The link between the Reynolds shear stress and the large structures of turbulent Couette-Poiseuille flow, Physics of Fluids 30 (2018) 041702.

[9] M. Lee, R. Moser, Extreme-scale motions in turbulent plane couette flows, Journal of Fluid Mechanics 842 (2018) 128–145.

[10] S. Pirozzoli, M. Bernardini, P. Orlandi, Large-scale motions and inner/outer layer interactions in turbulent Couette—Poiseuille flows, Journal of Fluid Mechanics 680 (2011) 534–563.

[11] S. Gandía-Barberá, La organización de las grandes escalas en flujos de pared, Master's thesis, ETSID, Universitat Politècnica de València, 2018. Content written in English, despite it has a Spanish title.

[12] M. J. Lee, J. Kim, The structure of turbulence in a simulated plane couette flow, Proceedings of the 8th Symposium on Turbulent Shear Flows, Munich (1991) 5.3.1–5.3.6.

[13] A. Ávila et al., Evidences of persisting thermal structures in couette flows, International Journal of Heat and Mass Transfer (2019). Still to be published.

[14] V. Avsarkisov, S. Hoyas, M. Oberlack, J. García-Galache, Turbulent plane Couette flow at moderately high reynolds number, Journal of Fluid Mechanics 751 (2014) R1.

[15] S. Kraheberger, S. Hoyas, M. Oberlack, Dns of a turbulent couette flow at constant wall transpiration up to $Re_\tau = 1000$, Journal of Fluid Mechanics 835 (2018) 421–443.

[16] M. Chong, A. Perry, B. Cantwell, A general classification of three-dimensional flow fields, Journal of Physics A. 2 (1990) 765–777.

[17] P. Chakraborty, S. Balachandar, R. Adrian, On the relationships between local vortex identification schemes, Journal of fluid mechanics 535 (2005) 189–214.

[18] J. C. del Álamo, J. Jiménez, P. Zandonade, R. Moser, Self-similar vortex clusters in the turbulent logarythmic region, Journal of Fluid Mechanics 561 (2006) 329–358.